



ELSEVIER

Journal of Contaminant Hydrology 48 (2001) 351–374

www.elsevier.com/locate/jconhyd

JOURNAL OF
**Contaminant
Hydrology**

Surfactant enhanced recovery of tetrachloroethylene from a porous medium containing low permeability lenses

2. Numerical simulation

Klaus M. Rathfelder ^a, Linda M. Abriola ^{a,*}, Tammy P. Taylor ^b,
Kurt D. Pennell ^b

^a *Department of Civil and Environmental Engineering, The University of Michigan, 1351 Beal Avenue,
Ann Arbor, MI 48109-2125, USA*

^b *School of Civil and Environmental Engineering, Georgia Institute of Technology, 200 Bobby Dodd Way,
Atlanta, GA 30332-0512, USA*

Received 9 December 1999; received in revised form 2 October 2000; accepted 30 October 2000

Abstract

A numerical model of surfactant enhanced solubilization was developed and applied to the simulation of nonaqueous phase liquid recovery in two-dimensional heterogeneous laboratory sand tank systems. Model parameters were derived from independent, small-scale, batch and column experiments. These parameters included viscosity, density, solubilization capacity, surfactant sorption, interfacial tension, permeability, capillary retention functions, and interphase mass transfer correlations. Model predictive capability was assessed for the evaluation of the micellar solubilization of tetrachloroethylene (PCE) in the two-dimensional systems. Predicted effluent concentrations and mass recovery agreed reasonably well with measured values. Accurate prediction of enhanced solubilization behavior in the sand tanks was found to require the incorporation of pore-scale, system-dependent, interphase mass transfer limitations, including an explicit representation of specific interfacial contact area. Predicted effluent concentrations and mass recovery were also found to depend strongly upon the initial NAPL entrapment configuration. Numerical results collectively indicate that enhanced solubilization processes in heterogeneous, laboratory sand tank systems can be successfully simulated using independently measured

* Corresponding author. Tel.: +1-734-764-9406; fax: +1-734-763-2275.
E-mail address: abriola@engin.umich.edu (L.M. Abriola).

soil parameters and column-measured mass transfer coefficients, provided that permeability and NAPL distributions are accurately known. This implies that the accuracy of model predictions at the field scale will be constrained by our ability to quantify soil heterogeneity and NAPL distribution. © 2001 Elsevier Science B.V. All rights reserved.

Keywords: Nonaqueous-phase liquids; Remediation; Surfactants; Numerical simulation; Tetrachloroethylene

1. Introduction

Remediation of aquifers contaminated by dense nonaqueous phase liquids (DNAPLs) is among the challenging problems facing hydrogeologists and engineers. The physical characteristics of most DNAPLs, including low aqueous solubility and high specific gravity, tend to limit their dissolution and recovery by hydraulic means, and make characterization of their subsurface distribution extremely difficult. Conventional pump-and-treat remediation methods are generally recognized to be inefficient for DNAPL recovery, requiring the injection and extraction of hundreds to thousands of pore volumes of water over long operating periods (National Research Council, 1994). Surfactant enhanced aquifer remediation (SEAR) is one of a number of promising innovative technologies that is being developed to address the problem of DNAPL contamination (Pennell and Abriola, 1998).

The feasibility of SEAR for the efficient removal of entrapped DNAPL from aquifer materials has been demonstrated in a number of laboratory column studies (Fountain et al., 1991; Pennell et al., 1993, 1994; Fortin et al., 1997; Kueper and Frind, 1991). Here DNAPLs have been recovered through enhanced solubilization and/or interfacial tension reductions that induce organic mobility. Many of these column studies have demonstrated that rate-limited NAPL solubilization and surfactant sorption can significantly influence SEAR performance (Pennell et al., 1993, 1994; Adeel and Luthy, 1995; Luning-Prak et al., 1996, 2000; Mason and Kueper, 1996; Abriola et al., 2000; Kueper and Frind, 1991). Field trials of SEAR technology have also produced promising results (Abdul et al., 1992; Abdul and Ang, 1994; Fountain, 1995; Fountain et al., 1996; Martel et al., 1998). Of particular concern in field-scale applications is the presence of subsurface heterogeneity that can significantly diminish recovery efficiency due to fluid bypassing of low permeability zones. Evidence of contaminant persistence has been documented in SEAR field trials (Fountain, 1995; Fountain et al., 1996). The potential influence of soil heterogeneity on SEAR performance has also been explored through mathematical simulations (Dekker and Abriola, 2000). Results of that study suggest that surfactant remediation efficiency will depend strongly on the spatial correlation structure and variance of the permeability distribution. Collectively, these previous studies indicate that efficient design and operation of field-scale SEAR applications necessitates an understanding of multiphase fluid flow and compositional transport in heterogeneous environments.

Mathematical models provide a platform for the integration of flow dynamics and transport processes, characterized at laboratory scales, with the spatial complexity of field settings. Such models may be used as tools for evaluating field-scale SEAR

applications, potentially leading to improved design and performance. Relatively few models, however, have been developed for simulation of field-scale SEAR applications. Models focusing on enhanced solubilization processes were developed by Wilson (1989) and Wilson and Clarke (1991). These models, while among the first enhanced solubilization simulators, were limited by assumptions of local equilibrium for NAPL solubilization and solute sorption. Abriola et al. (1993) developed a one-dimensional enhanced solubilization simulator that accounts for mass transfer rate limitations. Effluent data from enhanced solubilization experiments in laboratory soil columns (Pennell et al., 1993) were used to quantify interphase mass transfer rates and to verify the mathematical model. This formulation was later extended to two dimensions (Dekker, 1996; Dekker and Abriola, 2000). Among the most advanced SEAR simulators is the model of Delshad et al. (1996), based on an adaptation of an enhanced oil recovery simulator. This model has the ability to simulate surfactant-enhanced solubilization and organic liquid mobilization in three-dimensional systems (Brown et al., 1994).

This paper describes work directed towards the continued advancement and verification of numerical models for the simulation of multi-dimensional SEAR applications in heterogeneous porous media. The primary objective of this study is to assess the mathematical model formulation presented in Abriola et al. (1993) and Dekker and Abriola (2000) in terms of its ability to predict surfactant enhanced solubilization behavior in the multi-dimensional sand tank experiments described by Taylor et al. (2000). Following a presentation of the mathematical formulation, the numerical model is used to simulate column and sand box experiments. All system parameters for the two-dimensional sand tank simulations are independently measured or estimated from other laboratory observations. Model predictions are then evaluated through comparisons with observed effluent concentrations and contaminant recovery. Factors affecting numerical prediction accuracy, including mass transfer rate coefficients and initial organic liquid distributions, are also investigated.

2. Model description

2.1. Conceptual and mathematical formulation

The numerical simulator for enhanced solubilization processes employed herein is based on the formulation developed and implemented by Abriola et al. (1993) and Dekker and Abriola (2000). In their approach, the soil system is conceptualized as a saturated porous medium containing a mobile aqueous phase and an immobile organic liquid (NAPL). Micellar solubilization is assumed to be the sole organic recovery mechanism. This assumption is valid when the surfactant does not reduce the NAPL interfacial tension of the assumed NAPL residual to the point that organic liquid mobilization is initiated. This assumption is valid for the surfactant/NAPL/soil systems studied by Taylor et al. (2000). It is further conceptualized that the soil grains are continuously water-wet such that the organic liquid is surrounded by the aqueous phase. Sorption is consequently assumed to occur solely through the aqueous phase.

The mathematical development is based upon standard macroscopic phase and component mass balance relations. Flow of the aqueous phase is represented with a phase mass balance equation:

$$\frac{\partial}{\partial t}(n\rho_a s_a) = -\nabla(\rho_a q_a) + \sum_i E_{an}^i + \sum_i E_{am}^i \tag{1}$$

where the subscripts a, n, and m denote the aqueous, organic liquid (NAPL), and solid matrix phases, respectively, *n* is porosity, *s* is the fluid saturation, ρ is the phase mass density, *q* is the specific discharge, E_{an}^i and E_{am}^i are the rates of mass transfer of component *i* across the aqueous NAPL and aqueous-solid interphases, respectively, per unit volume of porous medium.

Under the assumption that NAPL removal occurs solely by micellar solubilization, the organic liquid phase mass balance equation is given as:

$$\frac{\partial}{\partial t}(n\rho_o s_n) = -\sum_i E_{an}^i \tag{2}$$

The fluid saturations in Eqs. (1) and (2) are related by the continuity constraint:

$$s_a + s_n = 1. \tag{3}$$

The composition of the aqueous and organic liquid phases varies temporally and spatially. For the specific application considered herein, the aqueous phase composition is tracked as a mixture of water, a single NAPL component, and surfactant. The transport of the latter two species within the aqueous phase is represented by:

$$\frac{\partial}{\partial t}(n s_a C_a^i) + \nabla(C_a^i q_a) - \nabla(n s_a D_H^i \nabla C_a^i) = E_{an}^i + E_{am}^i \tag{4}$$

where C_a^i is the mass concentration of component *i* in the aqueous phase (*i* = o, s for dissolved organic and surfactant components, respectively), and D_H^i is the hydrodynamic dispersion tensor of component *i*, evaluated as the sum of aqueous diffusion and mechanical dispersion terms (Bear, 1972). Partitioning of both surfactant and water into the organic liquid has been neglected for the simulations presented herein. The validity of this assumption has been confirmed for the selected organic-surfactant system: tetrachloroethylene (PCE)–polyoxyethylene (20) sorbitan monooleate (Tween 80) (Taylor et al., 2000).

Sorption of the surfactant and organic liquid components is expected to play a minor role in SEAR performance in the sand tank experiments described here due to the large surfactant concentration used and the relatively low organic carbon content of the sands. Generally, however, sorption can influence SEAR performance in field applications, and is therefore included in the model. For the sand tank application considered herein, equilibrium sorption of PCE is represented with a linear partitioning relationship, and equilibrium sorption of Tween 80 is assumed to conform to a Langmuir isotherm, as measured by Taylor et al. (2000):

$$S_m^s = \frac{S_{m,max}^s b C_a^s}{1 + b C_a^s} \tag{5}$$

Here S_m^s denotes the sorbed mass fraction of the surfactant components, $S_{m,max}^s$ is the maximum surfactant sorption, and b is a constant. Column studies of the transport of another nonionic surfactant (Triton X-100) in clean sands have indicated that sorption may be rate-limited (Adeel and Luthy, 1995). Accordingly, sorption of Tween 80 is modeled here as a nonequilibrium process using a linear driving force relationship:

$$(1 - n) \rho_m \frac{\partial S_m^s}{\partial t} = -K_e^{am} (C_{a,sat}^s - C_a^s) \quad (6)$$

where ρ_m is the solid particle mass density, K_e^{am} is the effective aqueous-solid mass transfer coefficient, and $C_{a,sat}^s$ is the aqueous phase concentration of surfactant in equilibrium with the solid phase loading as computed from the sorption isotherm (Eq. (5)). Surface diffusion of sorbed components is ignored.

The specific discharge of the aqueous phase is expressed in terms of a modified Darcy law:

$$q_a = \frac{k k_{ra}}{\mu_a} (\nabla P_a - \rho_a \mathbf{g}) \quad (7)$$

where k is the intrinsic permeability tensor; k_{ra} is relative permeability; μ_a is the dynamic viscosity; P_a is the fluid pressure, and \mathbf{g} is the gravitational acceleration vector. Here, the influence of the NAPL on the aqueous flow field is incorporated through the relative permeability, k_{ra} . This parameter is evaluated in the model as a unique function of aqueous saturation using the form of Brooks and Corey (1964):

$$k_{ra} = (\bar{s}_a)^{\frac{2+3\lambda}{\lambda}} \quad (8)$$

where $\bar{s}_a = (s_a - s_{ra}) / (1 - s_{ra})$ is the normalized saturation, s_{ra} is the residual aqueous phase saturation, and λ is the pore size index, an empirical parameter based upon fitting of moisture retention data.

Aqueous phase density and viscosity are, in general, composition-dependent. Aqueous phase density is computed in the model by Amagat's law (Reid et al., 1977), which assumes that the molar volumes of the mixture components are additive:

$$\rho_a = \frac{\sum_i x_a^i M^i}{\sum_i x_a^i M^i / \rho^i} \quad (9)$$

Here x_a^i is the aqueous phase component mole fraction, M^i is the component molecular weight, and ρ^i is the pure phase component mass density. The measured aqueous phase viscosity at constant temperature was found to be relatively insensitive to PCE concentration, but did vary as a function of surfactant concentration (Taylor et al., 2000). To model the sand tank experiments, the viscosity of the surfactant solution (Tween 80) at a given concentration is estimated by linear interpolation between the measured aqueous viscosity at 0% and 4% (wt.) at 22°C:

$$\mu_a = 0.9778 + 7.08 \times 10^{-6} C_a^s \quad (10)$$

where viscosity is in centipoise and aqueous phase concentration is in milligram per liter.

2.2. Solubilization modeling

Interphase mass transfer between the organic and aqueous phases is modeled as a nonequilibrium process using the linear driving force relation (Abriola et al., 1993; Taylor et al., 2000):

$$E_{an}^o = K_e^{an} (C_{a,sat}^o - C_a^o) \tag{11}$$

where $K_e = k_L a$ is the effective or overall aqueous-NAPL mass transfer coefficient, k_L is the aqueous controlled film mass transfer coefficient, a is the specific interfacial contact area between the NAPL and aqueous phases (area per unit volume of porous media), and $C_{a,sat}^o$ is the concentration of organic in equilibrium with the aqueous phase composition. The equilibrium concentration is evaluated as linear function of surfactant concentration as determined from batch experiments (Taylor et al., 2000):

$$C_{a,sat}^o = 150 + 0.67(C_a^s - C_{a,cmc}^s) \tag{12}$$

where concentration is expressed in milligram per liter.

Following the approach of Abriola et al. (1993) and Dekker and Abriola (2000), a relation for the effective mass transfer coefficient was developed from laboratory column effluent data. The effective mass transfer coefficient is expressed as the product of an initial effective mass transfer coefficient, determined from the effluent data, and an interfacial area reduction factor that accounts for diminishing interfacial area with decreasing NAPL saturation:

$$K_e = K_{e(i)} A \tag{13}$$

where $K_{e(i)} = k_{L(i)} a_{(i)}$ is the column- determined initial effective mass transfer rate; $k_{L(i)}$ is the initial film mass transfer coefficient; $a_{(i)}$ is the initial specific contact area; and $A = a/a_{(i)}$ is an interfacial area reduction factor.

The initial effective mass transfer rate coefficient, $K_{e(i)}$ is evaluated with empirical correlations developed from solubilization flushing experiments in laboratory soil columns (Taylor et al., 2000). Under flowing conditions, this mass transfer coefficient is related to the aqueous phase velocity:

$$K_{e(i)} = 0.0534 q_a^{0.712} \tag{14}$$

where q_a is the aqueous specific discharge in centimeter per hour and the mass transfer coefficient has units of liter per hour. During flow interruption periods, q_a is zero and Eq. (14) is therefore not applicable. Assuming the mass transfer coefficient remained constant during flow interruptions, Taylor et al. (2000) found that a best fit with effluent data was obtained with $K_{e,int(i)} = 0.016$ l/h, where $K_{e,int(i)}$ is the effective mass transfer rate during flow interruption conditions. Using effluent data obtained for a wide range of flow interrupt durations, Taylor et al. (2000) found that an improved model fit could be obtained if the mass transfer coefficient is expressed as a function of time:

$$K_{e,int(i)} = 0.0347(1 + t)^{-0.539} + 0.0051 \tag{15}$$

where t is time from the start of the interrupt in hour. Both constant- and time-dependent expressions for $K_{e,int(i)}$ were incorporated in the simulator.

To evaluate the interfacial contact area, the NAPL geometry is conceptualized as a fixed number of spherical blobs within each computational element (Dekker, 1996). The initial sphere diameters may be uniform or represented as a distribution of class sizes. From geometric considerations, the specific interfacial contact area is

$$a = \sum_j a^j = \sum_j f n s_n^j \frac{3}{r^j} \tag{16}$$

where j is the number of sphere classes, a^j is the specific interfacial contact are of the j th sphere class, s_n^j is the NAPL saturation in the j th sphere class, r^j is the sphere radius in the j th sphere class, and f is an empirical constant that accounts for the proportion of interfacial area in contact with mobile aqueous phase. In the absence of information, f is set to unity in this work. This assumption has no influence on model predictions reported herein, since the interfacial area reduction factor is independent of f (see Eq. 13).

At the start of each simulation, the initial contact area and the fixed number of NAPL spheres is initialized for each computational element. The initial contact area is evaluated from Eq. (16) and the number of NAPL spheres is evaluated with a volume balance, obtaining:

$$a_{(i)} = \sum_j f n s_{n(i)}^j \frac{3}{r_{(i)}^j} \tag{17}$$

$$N_j = \frac{n s_{n(i)}^j \mathbf{V}_{el}}{\frac{4}{3} \pi (r_{(i)}^j)^3} \tag{18}$$

where $s_{n(i)}^j$ and $r_{(i)}^j$ are the initial NAPL saturation and the initial sphere radius in the j th sphere class, N_j is the fixed number of NAPL spheres in the j th sphere class, and \mathbf{V}_{el} is the element volume.

The saturation of each NAPL sphere class is evaluated at the end of each time step using the solution from the NAPL mass balance expression (Eq. (2)) and the relation:

$$\frac{\partial s_n^j}{\partial t} = \frac{a^j}{a} \frac{\partial s_n}{\partial t} \tag{19}$$

Subsequently, the sphere radius is updated by rearranging Eq. (18);

$$r^j = \left[\frac{n s_n^j \mathbf{V}_{el}}{4 \pi N^j / 3} \right]^{1/3} \tag{20}$$

and the interfacial contact area is updated from Eq. (16). In the case of a single sphere class size, Eqs. (16), (18) and (20) can be used to obtain

$$A = \frac{a}{a_{(i)}} = \left(\frac{s_n}{s_{n(i)}} \right)^{2/3} \tag{21}$$

2.3. Model implementation

The model formulation presented above was implemented in a numerical simulator by modifying an existing two-dimensional multiphase flow and compositional transport simulator, MISER (Abriola et al., 1997). MISER solves the governing flow and transport equations in two space dimensions using a standard Galerkin finite element approach with linear triangular elements. The model has been verified mathematically through global mass balance computations, comparisons with one- and two-dimensional analytical solutions, and intermodel simulation comparisons (Abriola et al., 1997). The modified version of MISER was further verified through comparisons of enhanced solubilization predictions with those obtained by the SURF2D model presented in Dekker and Abriola (2000). A summary of the numerical algorithm over a single time step in MISER is as follows:

1. Using previous time step results, evaluate the aqueous/NAPL contact area with Eqs. (16) and (20), and update the aqueous phase viscosity (Eq. (10)) and relative permeability (Eq. (8)).
2. Iteratively solve the aqueous flow equation (Eq. (1)), and compute aqueous phase velocity (Eq. (7)).
3. Using concentration information for the current iterations, update the aqueous phase density (Eq. (9)), and evaluate the aqueous/NAPL effective mass transfer coefficient from (Eq. (13)) and the aqueous/solid interphase mass exchange as expressed in Eq. (6).
4. Sequentially solve aqueous phase transport equations (Eq. (4)) for the organic solute and surfactant components, the solid phase mass balance equation (Eq. (6)) for the organic solute and surfactant components, and the NAPL mass balance equation (Eq. (2)).
5. Increment iteration level and return to step 3 until convergence is established for aqueous and solid phase concentrations.
6. Update the aqueous phase saturation with Eq. (3) and update sphere class saturations using Eq. (19).

3. Model application

The modified MISER model was used to stimulate surfactant flush experiments described by Taylor et al. (2000). All parameters used in the simulations were determined by independent measurement or estimation. Porous medium and fluid properties are listed in Tables 1 and 2, respectively. Solubilization mass transfer coefficients were estimated from enhanced solubilization experiments in one-dimensional laboratory soil columns (Taylor et al., 2000). The simulation of these column experiments also provided an initial evaluation of model performance.

Table 1
Soil properties used in simulations

	Ottawa 20–30 sand	F-70 silica sand	Wurtsmith sand
<i>Soil characteristics</i>			
Porosity	0.33 ^a	0.41 ^b	0.33 ^c
Mean grain size (mm)	0.71 ^a	0.2 ^d	0.35 ^c
Intrinsic permeability (m ²)	3.9×10^{-10a}	8.19×10^{-12e}	4.2×10^{-11f}
Solid density (g/cm ³)	2.65 ^d	2.65 ^d	2.65 ^g
<i>PCE-water retention parameters</i>			
Brooks–Corey entry pressure (cm H ₂ O)	5.6 ^{a,h}	33.1 ^e	17.7 ^{c,h}
Brooks–Corey pore size index	3.46 ^a	3.3 ^e	6.1 ^c
Residual water saturation	0.07 ^a	0.189 ^e	0.125 ^c
Maximum entrapped PCE saturation	0.12 ⁱ	0.21 ^j	0.15 ^j
<i>Surfactant sorption parameters</i>			
Langmuir Q_{ms} (mg/g)	0.156 ^b	0.16 ^b	0.194 ^b
Langmuir b_s (l/mg)	0.010 ^b	0.029 ^b	0.008 ^b
Desorption rate coefficient k_d (l/h)	0.01 ^k	0.01 ^k	0.01 ^k
<i>PCE sorption parameters</i>			
Linear sorption coefficient (cm ³ /g)	0.08 ^l	0.3 ^l	0.17 ^m

^aPowers (1992).

^bTaylor et al. (2000).

^cDemond (1998).

^dU.S. Silica (1998).

^eKueper and Frind (1991).

^fEstimated from grain size data.

^gAssumed value.

^hScaled from air–water retention data.

ⁱPennell et al. (1996).

^jEstimated from permeability (Dekker, 1996).

^kPennell and Abriola (1998).

^lScaled by estimated interfacial area.

^mSorption to similar sands, Kibbey (1998).

Table 2
Fluid properties used in simulations

	PCE	Tween 80	4% Tween 80 solution
Density (g/cm ³)	1.62 ^a	1.08 ^b	1.002 ^c
Viscosity (cP)	0.90 ^a		1.261 ^c
Aqueous solubility (g/cm ³)	1.5×10^{-4d}		
Aqueous diffusivity (g/cm ³)	7.6×10^{-6e}	1.48×10^{-6b}	

^aKueper and Frind (1991).

^bDekker (1996).

^cTaylor et al. (2000).

^dVerschuere (1983).

^eAbriola et al. (1995).

3.1. Simulation of column flushing experiments

Taylor et al. (2000) describe five surfactant flush experiments conducted in 4.8 cm inside diameter laboratory soil columns packed with Ottawa 20–30 sand. Characteristics of the column flushing experiments are summarized in Table 3. Following the emplacement of residual PCE, each column was flushed with a 4% Tween 80 surfactant solution. Effluent PCE concentrations were measured over the course of the experiment. Flow interrupts were also performed to evaluate solubilization rates under no flow conditions.

The five column flushing experiments were simulated with the MISER model using mass transfer relations, Eqs. (14) and (15). Simulations were performed using either a single sphere size or a seven-class sphere size distribution. The latter distribution was based upon sieve analyses (mass proportion) of polymerized styrene that was entrapped at residual saturation levels in the Ottawa 20–30 sand (Powers, 1992). The column system was discretized into 200 triangular elements with nodal spacing of about 0.1 cm. No flow boundary conditions were implemented along the walls of the column, a constant mass flux (third type) condition was specified at the inlet, and a no dispersive flux boundary condition (second type) was implemented at the column outlet.

Measured and simulated PCE effluent concentrations for all five experiments are compared in Fig. 1. Visual inspection suggests good agreement was generally obtained during flowing conditions, especially prior to the first flow interrupt. Poorer agreement was obtained in the elution peaks following flow interrupts and during the flowing portion following the interrupts in columns 3 and 4. The overall downward trend in effluent concentrations was captured with the diminishing sphere model that incorporated an interfacial area reduction factor.

For comparative purposes, agreement between measured and predicted effluent concentrations was also quantified by an average absolute normalized deviation defined by:

$$\overline{\text{diff}} = \frac{\sum_{n_m} \text{abs}(C_{a(m)}^o - C_{a(p)}^o)}{n_m C_{a,\text{sat}}^o} \quad (22)$$

where $C_{a(m)}^o$ and $C_{a(p)}^o$ are the measured and predicted effluent concentrations, respectively, and n_m is the number of measured effluent concentrations. Average absolute normalized deviations from the five column experiments (Table 4) ranged between a

Table 3
Summary of column experiments

	Column 1	Column 2	Column 3	Column 4	Column 5
Length (cm)	10.2	9.6	9.9	10.0	10.0
Porosity	0.341	0.348	0.346	0.340	0.345
Pore volume (cm ³)	62.94	60.45	61.98	61.52	62.43
Initial PCE saturation	0.1128	0.096	0.1357	0.1070	0.1087
Flow rate (cm ³ /min)	1.0	2.5	0.25	1.25	1.5
Flow interrupt duration (h)	14.17	24.45	50	43	8.33

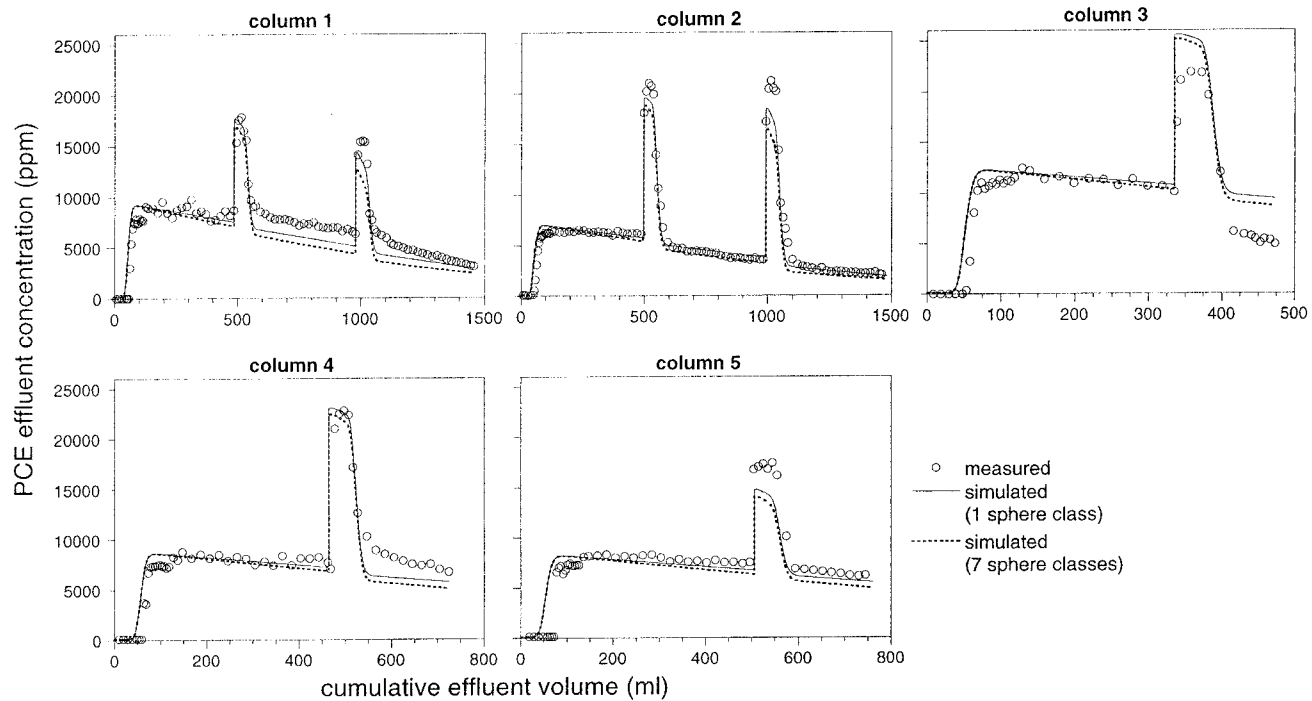


Fig. 1. Measured and predicted PCE effluent concentrations as a function of cumulative effluent volume from five surfactant flush column experiments.

Table 4

Average absolute normalized deviations in effluent concentrations predicted in the simulation of the five column experiments

	Column 1	Column 2	Column 3	Column 4	Column 5
Single sphere class	0.046	0.031	0.076	0.051	0.057
Seven sphere class	0.062	0.041	0.068	0.056	0.067

low of 0.031 in column 2 and a high of 0.076 in column 3. Note that the average absolute normalized deviation is based upon data from the entire column flush experiment and is most influenced by large deviations in the initial breakthrough period and during the elution peaks.

Effluent concentration predictions using the seven-sphere class NAPL distribution were slightly lower than corresponding concentrations obtained with a single sphere class distribution. The lower PCE effluent concentrations are a consequence of a more rapid change in interfacial area. A more rapid change in the area reduction factor (A) was observed with the seven-class distribution because it was dominated by the smaller sphere sizes, which contain a greater area to volume ratio. Predictions obtained with the seven-sphere class distribution exhibit small visual deviations from those with the single sphere class distribution (Fig. 1), and in four out of five cases had a larger mean absolute normalized deviation (Table 4). For these reasons, the seven-sphere class distribution was not employed in subsequent simulations.

Efforts were made to improve predictions during the elution peaks. Results in Fig. 1 were obtained using Eq. (15) to estimate the initial effective mass transfer coefficient during the flow interrupt period, resulting in an over-prediction in the elution peak height for the longest interrupt duration (50 h in column 3) and an under-prediction in the elution peak height for the shortest interrupt duration (8.3 h in column 5). Recall that Taylor et al. (2000) did not consider interfacial area reduction prior to the flow interruption in their development of the flow interruption mass transfer expression, Eq. (15), assuming this change to be negligible for the early time flow interruptions. An alternative time-dependent expression for the mass transfer coefficient, however, can be developed that accounts for this preceding area reduction. In this approach, an initial mass transfer coefficient is evaluated with Eq. (13), where the value of A immediately prior to a flow interruption is determined from Eq. (21) using the average PCE saturation at that time (the PCE volume reduction prior to the flow interrupts varied between 22% and 30% in the columns). Using this approach, the following modified mass transfer correlation for flow interruptions can be developed:

$$K_{e,int(i)} = 0.038(1 + t)^{-0.539} + 0.009. \quad (23)$$

Fig. 2 compares predicted PCE effluent concentrations for column 5 using three alternative approaches to express the flow interrupt mass transfer coefficient (a constant value, Eqs. (15) and (23)). Results show that an improvement in the match of the elution peak height can be obtained when Eq. (23) is employed for flow interrupt (Eq. (15))

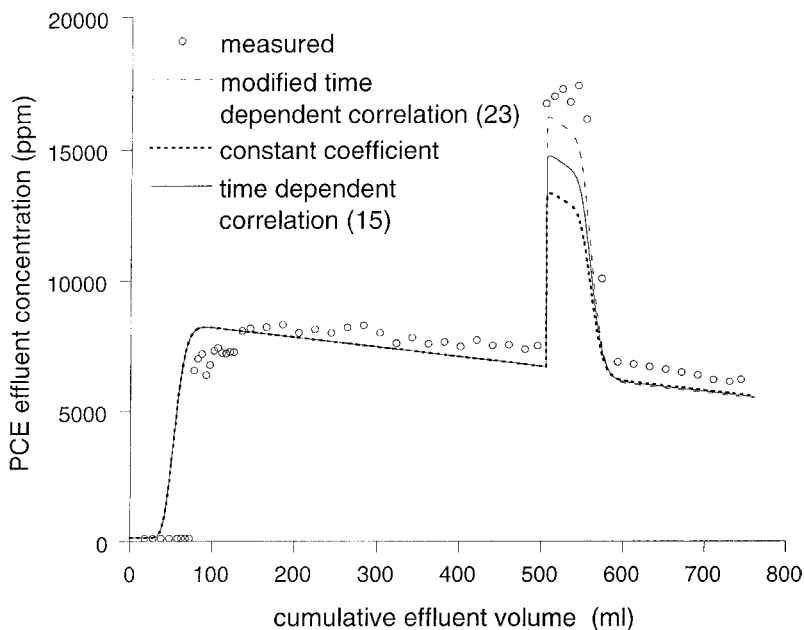


Fig. 2. Comparison of predicted effluent concentrations in column 5 using alternative mass transfer correlations for flow interrupt conditions.

conditions. Mean absolute normalized deviations using the constant mass transfer value, Eq. (15), and Eq. (23) were 0.061, 0.057, and 0.053, respectively.

The importance of using system calibrated mass transfer coefficients is illustrated in Fig. 3. Here, PCE effluent concentration predictions are compared for column 2 experimental conditions using four alternative mass transfer correlation expressions: a correlation based upon dodecane solubilization experiments (Abriola et al., 1993), a correlation developed for NAPL dissolution (Powers, 1992), the PCE correlation given by Eqs. (14) and (15), and this same correlation ignoring the interfacial area reduction (i.e., $A = 1$). Examination of Fig. 3 reveals that near equilibrium effluent concentrations are predicted with the NAPL dissolution correlation. The predicted concentrations are substantially greater than the measured values and, consequently, use of this correlation results in an overly optimistic prediction of PCE recovery. In contrast, simulations using the dodecane correlation exhibit an under-prediction of effluent concentrations over the majority of the experiment, consistent with the much slower rates of dodecane micellar solubilization (Pennell et al., 1993) in comparison with those observed for PCE. The dependence of mass transfer behavior on NAPL and surfactant characteristics was examined by Luning-Prak et al. (2000). Predictions using the PCE correlation exhibit a close match with measured values. However, failure to incorporate interfacial area reduction results in increasing deviations from measured values with time. Effluent tailing behavior is not accurately captured if area reduction is neglected, resulting in an unrealistic estimate of the time necessary for complete PCE recovery. Collectively, these

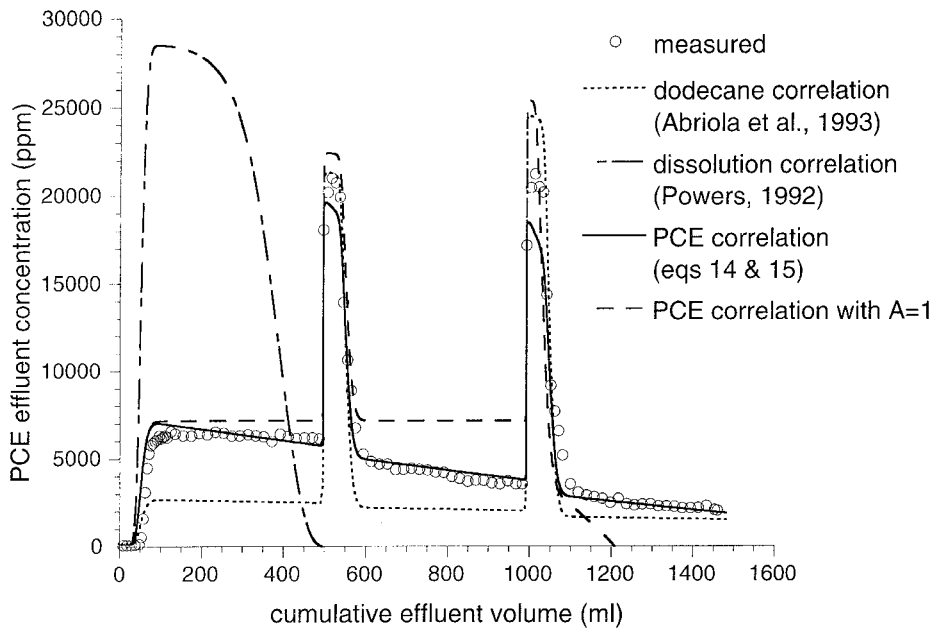


Fig. 3. Comparison of predicted effluent concentrations in column 2 using alternative mass transfer correlations.

simulations demonstrate that the accurate prediction of enhanced solubilization requires the incorporation of rate-limited solubilization processes, the quantification of system-dependent interphase mass transfer rates, and the explicit representation of interfacial contact area or a saturation-dependent mass transfer coefficient.

3.2. Simulation of two-dimensional flushing experiments

Taylor et al. (2000) describe two enhanced solubilization experiments conducted in a two-dimensional laboratory sand tank containing three different sands. The coarsest sand (Ottawa 20–30) was used as the background material, with less permeable ‘macro-heterogeneities’ embedded within it as rectangular-shaped lenses. The general configuration of the sand tank system is shown in Fig. 4 and experimental conditions are summarized in Table 5. A known quantity of PCE was injected into the tank at a constant flow rate and allowed to drain and redistribute. Nonreactive tracer tests were performed before and after the PCE release. Following PCE redistribution, the tank was flushed with 4% Tween 80 surfactant solution at a fairly constant flow rate. Effluent concentrations of PCE and surfactant were measured over the course of the experiment.

The sand tank experiments were simulated with the MISER model. The simulation domain incorporated the actual size and location of the sand lenses, which varied slightly between the two experiments. In model simulations, the sand lenses were assumed to be perfectly rectangular. The vertical ends of the sand tank were screened

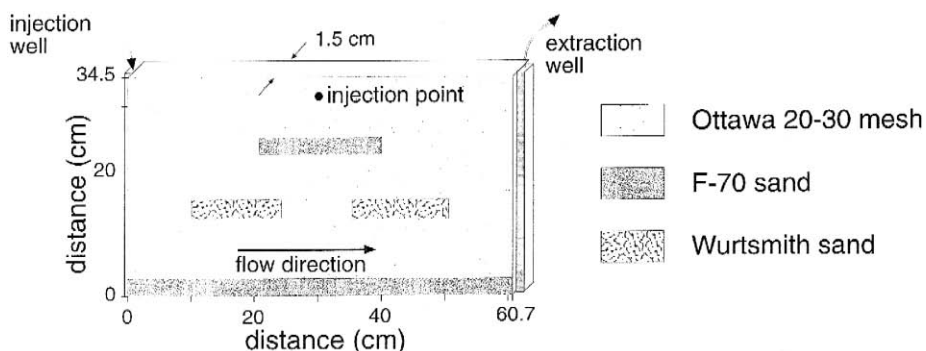


Fig. 4. Numerical domain used in sand box simulations.

over the entire thickness and hydraulically connected to influent and effluent well chambers ($1 \times 1.5 \times 34$ cm). The fluids were introduced and withdrawn through Teflon tubes placed within the well chambers. Because of significant mixing within the well chambers, these regions were included in the simulation domain and modeled as a high permeability porous medium ($k = 1.0 \times 10^{-9} \text{ m}^2$, $n = 1.0$). The entire tank domain was discretized into approximately 6700 triangular elements (3500 nodes). Horizontal and vertical nodal spacing ranged from 0.5 to 1.1 cm, with the majority of nodes spaced about 1.0 cm apart.

No flow boundary conditions were specified along the entire tank boundary. Influent conditions were simulated as a time-dependent mass flux (third type condition for the transport equations) specified at a single node corresponding to the depth of the Teflon tube placed in the influent chamber. The influent flow rate was time varying, corresponding to the measured average discharge within each effluent collection period. The influent concentrations were specified as 4% Tween 80 and zero PCE concentration. Effluent conditions were simulated with a constant head condition at a single node corresponding to the depth of the Teflon tube placed in the effluent chamber. Second type (no dispersive flux) conditions were implemented at this node for the transport equations.

A major constraint of the modeling effort was the inability to accurately characterize the initial PCE distribution prior to initiation of the surfactant flush. Two approaches

Table 5
Conditions of the laboratory sand tank surfactant flushing experiments

	Box A	Box B
Total pore volume (ml)	1104	1041
Effective PCE volume (ml)	38.05	18.54
Average PCE injection rate (ml/h)	20.0	18.9
Approximate PCE redistribution period (h)	36	72
Average surfactant solution injection rate (ml/min)	3.95	0.91
Flow interrupt durations (h)	14.9, 15.2, 14.7	22.9, 18.8

were used to specify the initial PCE distribution in an effort to develop realistic initial conditions and to test the influence of the initial distribution on simulation results. In the first approach, an initial PCE distribution was developed from visual observations by qualitatively dividing the visual limits of the dyed PCE into regions of constant saturation. These initial PCE distributions are shown in Fig. 5 and are referred to as the “visual distribution”. The total PCE mass in the visual distributions agrees to within 0.5 ml of the injected mass. In the second approach, the initial PCE distributions were developed by simulating the PCE infiltration and redistribution event using a two-dimensional immiscible flow simulator, M-VALOR (Abriola et al., 1992). These initial PCE distributions are also shown in Fig. 5 and are referred to as the “simulated distributions”. The visual and simulated distributions exhibit distinct differences. The configurations of the PCE pools on the fine sand lenses are symmetric in the simulated distributions because lenses were simulated as regular and horizontal. In reality, the lenses were slightly irregular and tilted, resulting in greater mass movement towards one end of the tank. A second major differences between simulated and observed PCE distributions is that horizontal spreading within flow paths between the lenses and in the pooled regions is greater in the simulated case.

Tracer tests with potassium iodide conducted in Box A (Taylor et al., 2000) were initially simulated with MISER to verify the predicted flow field and to calibrate dispersivity coefficients using a trial and error matching procedure. Fig. 6 compares the measured and simulated tracer breakthrough curves using constant longitudinal and transverse dispersivities of 0.1 and 0.01 cm, respectively. As anticipated from the scale of the sand tank experiment, the fitted longitudinal dispersivity value (0.1 cm) is about double the values (0.038–0.065 cm) measured by Taylor et al. (2000) in column tracer tests in 20–30 mesh Ottawa sand. The fitted dispersivity values were applied uniformly to all sands; no attempt was made to fit soil dependent dispersivities because it was presumed that the flow regime was controlled by the background 20–30 Ottawa sand. Additionally, no attempt was made to modify dispersivity values for the presence of NAPL saturation. Simulations for the post-entrapment tracer test presented in Fig. 6 were obtained with the visual PCE distribution shown in Fig. 5. Slightly more dispersion and later breakthrough was predicted than actually observed. This discrepancy is most likely due to differences between the actual and simulated initial entrapment configuration. Overall, however, the simulated tracer breakthrough curves agree reasonably well with the observed breakthrough curves.

Surfactant flushing experiments in Boxes A and B were simulated using the PCE distributions shown in Fig. 5 and mass transfer relations developed from the column experiments (Eqs. (14) and (15)) with a single sphere class distribution. Measured and predicted effluent concentrations and PCE recovery are compared in Fig. 7. Examination of this figure reveals a variation in the extent of deviations between measured and predicted effluent concentrations over the duration of the experiment. The figure also suggests that these deviations depend on the assumed initial PCE distribution. Comparisons of cumulative PCE recovery in Fig. 7 reveal that PCE recovery in Box A was under-predicted with a maximum deviation at the end of the experiment of 33.1% and 39.6% using the visual and simulated PCE distributions, respectively. Better agreement between predicted and measured PCE recovery was obtained for Box B with a

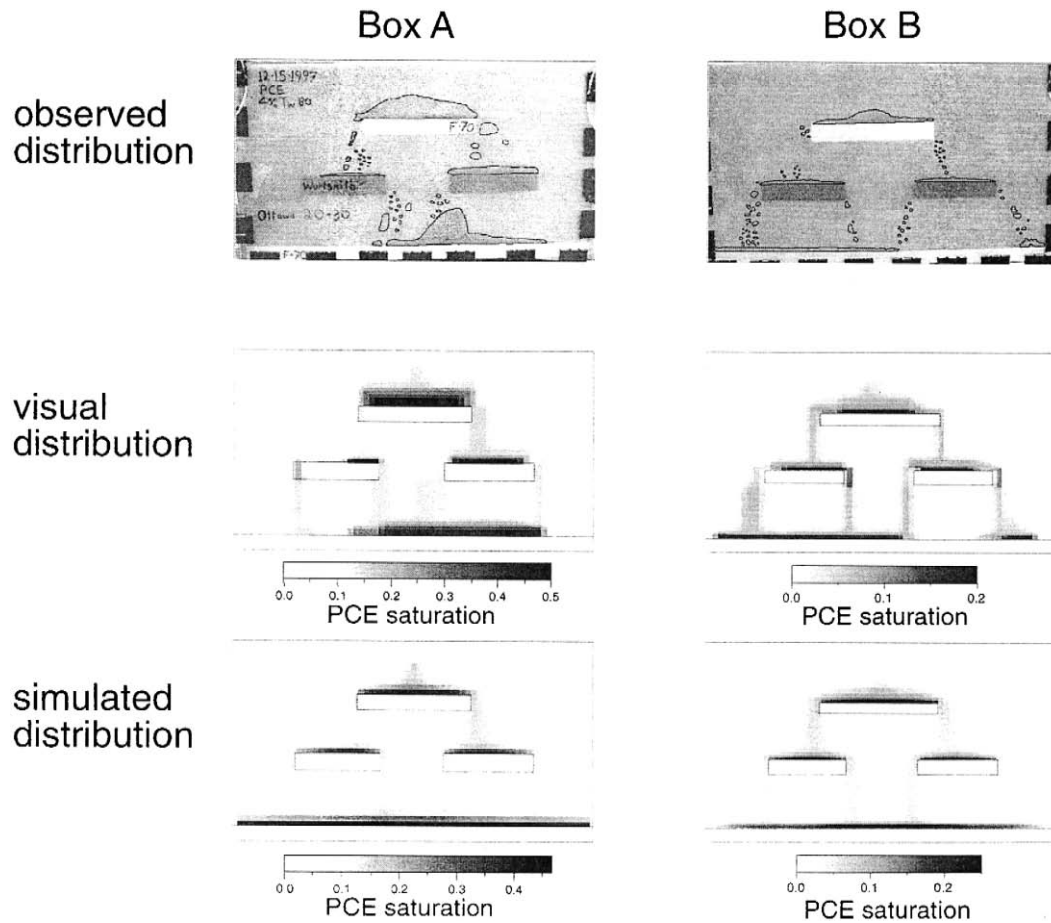


Fig. 5. Comparison of observed and initial PCE distributions used in model simulations.

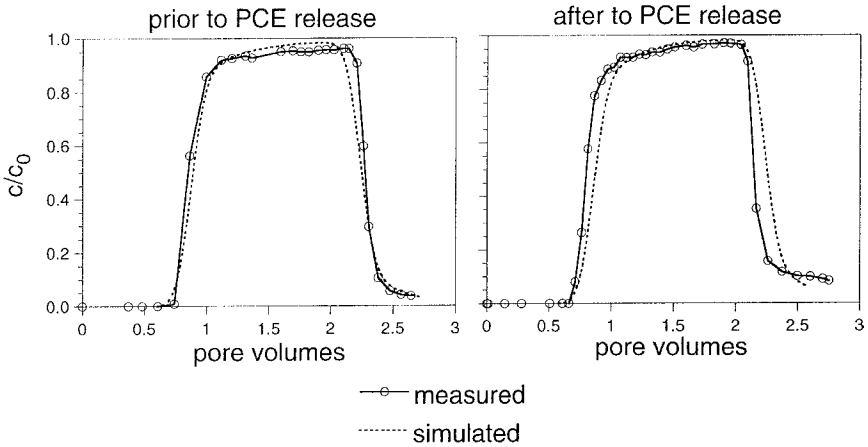


Fig. 6. Measured and simulated tracer breakthrough curves in box A.

maximum deviation at the end of the experiment of 0.04% and 7.9% using the simulated and visual PCE distributions, respectively. In both experiments, predictions using the visual PCE distribution generally gave better agreement with observed PCE recovery, than did those using simulated distributions. A comparison of measured and predicted surfactant effluent concentrations is also shown in Fig. 7. Generally, good agreement was obtained for both boxes, although the slope of the observed breakthrough in Box B was steeper than was predicted by the simulator. Predicted surfactant effluent concentrations were minimally influenced by surfactant sorption, as determined by comparison with the simulated breakthrough of a non-sorbing surfactant.

Experimental observations suggest that discrepancies between the observed and predicted effluent concentrations may be largely attributed to variations between the actual and assumed initial PCE distributions. Visual observation of PCE removal during the surfactant flush indicated that PCE was removed first along unobstructed horizontal flow paths between the inlet and outlet chambers (i.e. above, below, and between the lenses), followed by a gradual shrinkage of the thickness of the NAPL pools above the lenses. Therefore, PCE recovery during early periods was largely controlled by the NAPL volume and distribution along the unobstructed horizontal flow paths above the pooled regions, and late time recovery was largely controlled by the NAPL volume and distribution within the pooled regions.

Fig. 7 shows that effluent concentrations within the initial breakthrough periods were over-predicted with slightly better predictions obtained using the visual PCE distributions. An over-prediction in effluent concentration suggests that the NAPL contact area above the pooled regions (i.e. horizontal path length through the zone of residual NAPL) was overestimated due to the assumed initial PCE distributions. Fig. 5 shows that the horizontal path length through the NAPL above the pooled regions is greater for the simulated PCE distribution, which could account for the poorer predictions obtained with this initial distribution. Effluent concentrations following the initial PCE breakthrough (Fig. 7) are generally under-predicted, suggesting an insufficient NAPL volume

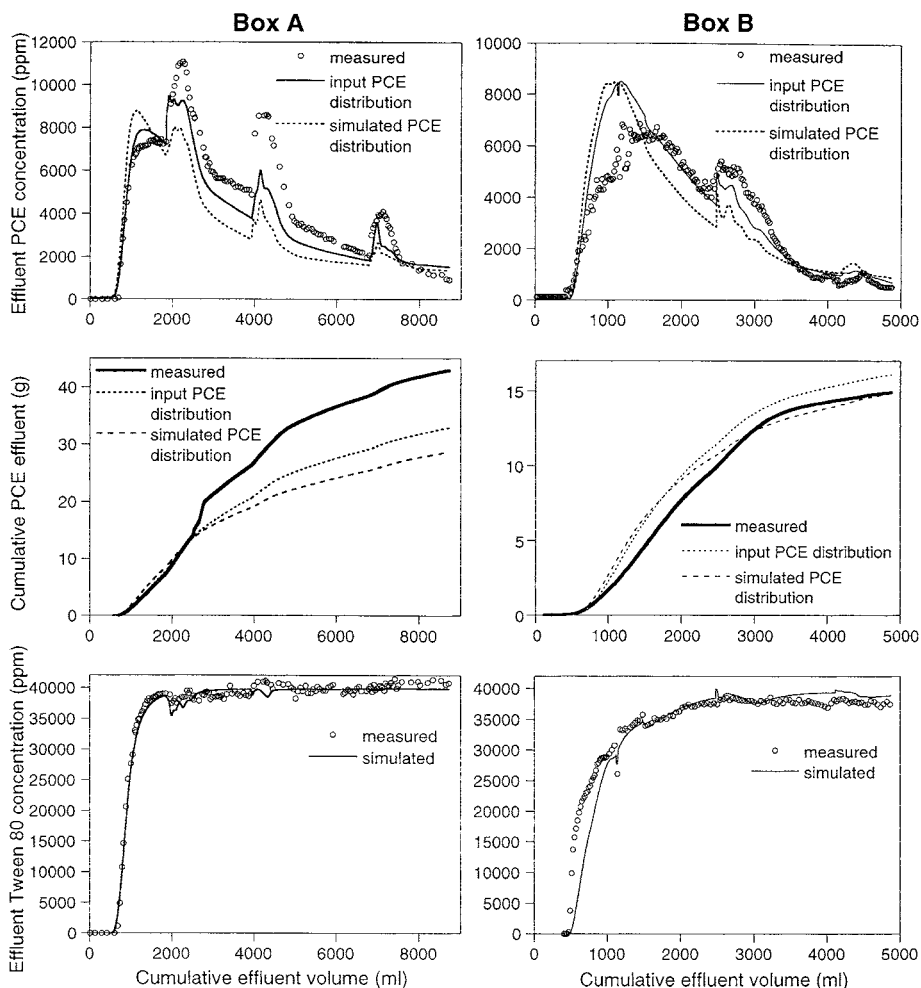


Fig. 7. Comparison of measured and simulated effluent concentrations and PCE recovery from sand tank surfactant flush experiments.

or contact are within the horizontal flow paths in the model. During late time periods, predicted effluent concentrations agree reasonably well with observed concentrations, suggesting that the NAPL volume and contact area in the pooled regions was adequately represented by both initial PCE distributions.

Effluent PCE concentration peaks following flow interruptions tended to be under-predicted in most cases. Comparisons with simulation results using a constant mass transfer coefficient (not shown) revealed that the functional form of the flow interruption mass transfer expression did not significantly alter predictions of effluent concentrations. The maximum PCE concentration in the elution peak following flow interruptions appears to be most sensitive to the PCE distribution prior to the start of the interruption.

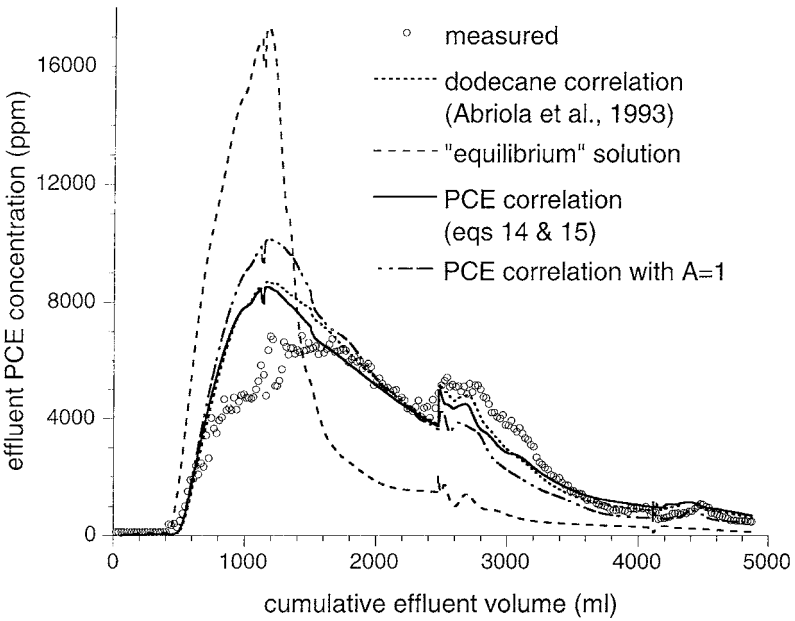


Fig. 8. Comparison of predicted effluent concentrations from the simulation of the Box B experiment using alternative mass transfer correlations.

The sensitivity of predicted effluent concentrations to the effective aqueous-NAPL mass transfer coefficients is further examined in Fig. 8. Here, comparisons for the model simulations of Box B experiment are shown for four interphase mass transfer correlation expressions: the dodecane correlation (Abriola et al., 1993), the PCE correlation (Taylor et al., 2000) wherein interfacial area reduction is ignored ($A = 1$), and an “equilibrium” solution obtained using the dissolution correlation (Powers, 1992) during flowing conditions and a large mass transfer coefficient during the flow interrupts. Effluent concentrations predicted with the dissolution correlated exhibit a large disparity with measured data during the initial break-through period. Note that the maximum concentration attained is less than the saturated concentration due to dilution effects. After the initial breakthrough period, predicted effluent concentrations for this “equilibrium” simulation fall below observed concentrations due to the initial over-prediction of NAPL removal and the consequent over-prediction of the reduction in NAPL contact area. Similar behavior is observed when the PCE measured correlation is employed but interfacial area reduction is ignored. Here, increased mass transfer coefficients result in the over-prediction of effluent concentrations at early times, followed by the under-prediction of PCE effluent concentrations at late times. Simulations obtained using the dodecane correlation exhibit solution behavior similar to that obtained using the PCE correlation. This is attributed to fact that the PCE and dodecane correlations predict similar mass transfer coefficients at low velocities, but exhibit increasing disparity at higher velocities, as shown previously in the column results (Fig. 3). Collectively, these

results further emphasize the need for measurement of system-dependent mass transfer correlations to accurately predict NAPL recovery at this scale.

4. Summary and conclusions

An improved solubilization simulator, based on the formulation of Abriola et al. (1993), was used to simulate surfactant enhanced solubilization experiments in laboratory soil columns and sand tanks. Simulation results exhibited reasonable agreement with measured PCE and surfactant effluent concentrations and PCE recovery. Additional simulations were performed to evaluate the influence of the mass transfer coefficient and the initial PCE distribution on prediction accuracy. Results from simulations of surfactant enhanced solubilization in laboratory column and sand tank experiments support the following conclusions.

(1) The model formulation of enhanced solubilization presented by Abriola et al. (1993) is applicable for simulation of enhanced solubilization processes in multi-dimensional heterogeneous systems.

(2) Accurate prediction of enhanced solubilization processes requires the simulations of rate-limited dissolution processes, the quantification of system-dependent interphase mass transfer rates, and the explicit representation of interfacial contact area or a saturation-dependent mass transfer coefficient.

(3) Column-measured mass transfer coefficients can be used successfully for the prediction of large-scale experiments.

(4) Accurate prediction of NAPL recovery in the two-dimensional systems depends on the knowledge of the initial NAPL entrapment configuration, which in turn is strongly influenced by soil heterogeneity.

These findings suggest that numerical models can be successfully used to predict and assess enhanced solubilization processes in field systems, provided that system heterogeneity and NAPL distribution can be adequately specified and that laboratory-scale mass transfer coefficient correlations are available. Future research should be directed towards the development and validation of interphase mass transfer relations for a variety of soil/organic/surfactant systems, and towards the validation of simulations for NAPL entrapment in heterogeneous systems.

Notation

a	specific interfacial contact area [L^{-1}]
A	interfacial area reduction factor
b	Langmuir sorption constant [$L^3 M^{-1}$]
C	mass concentration [$M L^{-3}$]
$C_{a,cmc}$	aqueous phase concentration at the CMC [$M L^{-3}$]
$C_{a,sat}$	saturated aqueous phase concentration [$M L^{-3}$]
D_H	hydrodynamic dispersion tensor [$L^2 T^{-1}$]
E	interphase mass transfer rate [$M L^{-3} T^{-1}$]
f	interfacial area fraction in contact with mobile aqueous phase
g	gravitational acceleration [$L T^{-2}$]

k	intrinsic permeability [L^2]
k_L	liquid film mass transfer coefficient [$L T^{-1}$]
k_{ra}	aqueous phase relative permeability
K_e	effective mass transfer coefficient [T^{-1}]
λ	pore size index
M	molecular weight [$M mol^{-1}$]
N	number of spheres
n	porosity
n_m	number of measured data points
P	phase pressure [$M L^{-1} T^{-2}$]
q	specific discharge [$L T^{-1}$]
r	sphere radius [L]
s	fluid saturation
s_{ra}	aqueous residual saturation
S	sorbed mass fraction
$S_{m,max}$	Langmuir maximum sorption capacity
t	time [T]
μ	dynamic viscosity [$M L^{-1} T^{-1}$]
ρ	mass density [$M L^{-3}$]
V_{el}	volume of computational element [L^3]
x	component mole fraction

Subscripts and superscripts

a	aqueous phase
i	phase component
(i)	initial time
j	sphere size class
m	solid phase
(m)	measured
n	organic liquid phase
o	dissolved organic component
(p)	predicted
s	surfactant component

Acknowledgements

Funding for this research was provided by the US Environmental Protection Agency, Great Lakes and Mid-Atlantic Center for Hazardous Substance Research (GLMAC-HSRC) under Grant No. R-825540 and by the US Environmental Protection Agency, Office of Research and Development under Grant No. R-825409. Additional matching funds were provided to the GLMAC-HSRC by the Michigan Department of Environmental Quality. The content of this publication does not necessarily represent the views of either agency and has not been subject to agency review.

References

- Abriola, L.M., Rathfelder, K., Yadav, S., Maiza, M., 1992. VALOR Code Version 1.0: A PC Code for Simulating Subsurface Immiscible Contaminant Transport. EPRI TR-101018, Electric Power Research Institute, Palo Alto.
- Abriola, L.M., Dekker, T.J., Pennell, K.D., 1993. Surfactant-enhanced solubilization of residual dodecane in soil columns: 2. Mathematical modeling. *Environ. Sci. Technol.* 27 (12), 2341–2351.
- Abriola, L.M., Pennell, K.D., Pope, G.A., Dekker, T.J., Luning-Prak, D.J., 1995. Impact of surfactant flushing on the solubilization and mobilization of dense nonaqueous-phase liquids. In: Sabatini, D.A., et al. (Eds.), *Surfactant-Enhanced Subsurface Remediation: Emerging Technologies*. ACS Symposium Series No. 594. American Chemical Society, Washington, DC, pp. 10–23.
- Abriola, L.M., Lang, J.R., Rathfelder, K.M., 1997. Michigan Soil Vapor Extraction Remediation (MISER) Model: a computer program to model soil vapor extraction and bioventing of organic chemicals in unsaturated geologic materials, U.S. Environmental Protection Agency, EPA/600/R-97/099, National Risk Management Research Laboratory, Ada, OK.
- Abriola, L.M., Condit, W.E., Cowell, M.A. et al., 2000. Investigation of the influence of soil texture on rate-limited micellar solubilization. *J. Environ. Eng.* 126 (1), 39–46.
- Abdul, A.S., Ang, C.C., 1994. In situ surfactant washing of polychlorinated biphenyls and oils from a contaminated field site: Phase II pilot study. *Ground Water* 32 (5), 727–734.
- Abdul, A.S., Gibson, T.L., Ang, C.C., Smith, J.C., 1992. In situ surfactant washing of polychlorinated biphenyls and oils from contaminated soils. *Ground Water* 30, 219–231.
- Adeel, Z., Luthy, R.G., 1995. Sorption and transport kinetics of a nonionic surfactant through an aquifer sediment. *Environ. Sci. Technol.* 29, 1032–1042.
- Bear, J., 1972. *Dynamics of Fluids in Porous Media*. Elsevier, New York.
- Brooks, R.H., Corey, A.T., 1964. Hydraulic properties of porous media, *Hydrol. Paper No. 3*, Colorado State University, Fort Collins.
- Brown, C.L., Pope, G.A., Abriola, L.M., Sepehrnoori, K., 1994. Simulation of surfactant-enhanced aquifer remediation. *Water Resour. Res.* 30 (11), 2959–2977.
- Delshad, M., Pope, G.A., Sepehrnoori, K., 1996. A compositional simulator for modeling surfactant enhanced aquifer remediation: 1. Formulation. *J. Contam. Hydrol.* 23, 303–327.
- Diamond, A.H., 1998. Personal communication, University of Michigan, Ann Arbor, Michigan.
- Dekker, T.J., 1996. An Assessment of the Effects of Field-Scale Formation Heterogeneity on Surfactant Aquifer Remediation. PhD Dissertation, The University of Michigan, Ann Arbor, Michigan.
- Dekker, T.J., Abriola, L.M., 2000. The influence of field-scale heterogeneity on the surfactant-enhanced remediation of entrapped nonaqueous phase liquids. *J. Contam. Hydrol.* 42, 187–218.
- Fortin, J., Jury, W.A., Anderson, M.A., 1997. Enhanced removal of trapped non-aqueous phase liquids from saturated soil using surfactant solutions. *J. Contam. Hydrol.* 24, 247–267.
- Fountain, J.C., Waddell-Sheets, C., Lagowski, A., Taylor, C., Frazier, D., Byrne, M., 1995. Enhanced removal of dense nonaqueous phase liquids using surfactants: capabilities and limitations of field trials. In: Sabatini, D.A., et al. (Eds.), *Surfactant-Enhanced Subsurface Remediation: Emerging Technologies*. ACS Symposium Series No. 594. American Chemical Society, Washington, DC, pp. 177–190.
- Fountain, J.C., Klimek, A., Beikirch, M.G., Middleton, T.M., 1991. Use of surfactants for in situ extraction of organic pollutants from a contaminated aquifer. *J. Hazard. Mater.* 38 (3), 295–311.
- Fountain, J.C., Starr, R.C., Middleton, T., Beikirch, M., Taylor, C., Hodge, D., 1996. Controlled field test of surfactant-enhanced aquifer remediation. *Ground Water* 34 (5), 910–916.
- Kibby, T., 1998. Personal communication, University of Michigan, Ann Arbor, Michigan.
- Kueper, B.H., Frind, E.O., 1991. Two-phase flow in heterogeneous porous media: 1. Model development. *Water Resour. Res.* 27 (6), 1049–1057.
- Luning-Prak, D.J., Pennell, K.D., Abriola, L.M., Weber, W.J., 1996. Rate controlled micellar solubilization of an LNAPL in aquifer materials. In: Lakshmi, R.N. (Ed.), *Proc. of the ASCE Specialty Conference on Nonaqueous Phase Liquids in the Subsurface Environment*. American Society of Civil Engineers, Washington, DC, pp. 639–648.
- Luning-Prak, D.J., Abriola, L.M., Weber, W.J., Bocskey, K.A., Pennell, K.D., 2000. Solubilization rates of *n*-alkanes in micellar solutions of nonionic surfactants. *Environ. Sci. Technol.* 34, 476–482.

- Martel, R., Gelinis, P.J., Saumure, L., 1998. Aquifer washing by micellar solutions: 3. Field test at the Thouin sand pit. *J. Contam. Hydrol.* 30, 33–48.
- Mason, A.R., Kueper, B.H., 1996. Numerical simulation of surfactant enhanced solubilization of pooled NAPL. *Environ. Sci. Technol.* 30 (11), 3205–3215.
- National Research Council, 1994. *Alternatives for Ground Water Cleanup*. National Academy Press, Washington, DC.
- Pennell, K.D., Abriola, L.M., 1998. Surfactant-enhanced aquifer remediation: fundamental processes and practical applications. In: Sikdar, S.K., Irvine, R.L. (Eds.), *Bioremediation: Principles and Practice*, vol. 1. Technomic Publ., Lancaster, PA, pp. 693–750.
- Pennell, K.D., Abriola, L.M., Weber, W.J., 1993. Surfactant-enhanced solubilization of residual dodecane in soil columns. 1. Experimental investigation. *Environ. Sci. Technol.* 27 (12), 2232–2240.
- Pennell, K.D., Jin, M., Abriola, L.M., Pope, G.A., 1994. Surfactant enhanced remediation of soil columns contaminated by residual tetrachloroethylene. *J. Contam. Hydrol.* 16 (10), 35–53.
- Pennell, K.D., Pope, G.A., Abriola, L.M., 1996. Influence of viscous and buoyancy forces on the mobilization of residual tetrachloroethylene during surfactant flushing. *Environ. Sci. Technol.* 30 (4), 1328–1335.
- Powers, S.E., 1992. *Dissolution of Nonaqueous Phase Liquids in Saturated Subsurface Systems*. PhD Dissertation, University of Michigan, Ann Arbor, Michigan.
- Reid, R.C., Prausnitz, J.M., Sherwood, T.K., 1977. *The Properties of Gases and Liquids*. McGraw-Hill, New York.
- Taylor, T.P., Pennell, K.D., Abriola, L.M., Dane, J.H., 2000. Surfactant enhanced recovery of tetrachloroethylene from a porous medium containing low permeability lenses: 1. Experimental studies. *J. Contam. Hydrol.* this issue.
- U.S. Silica, 1998. *Product Data Sheets*. Berkeley Spring, WV.
- Verschueren, K., 1983. *Handbook of Environmental Data on Organic Chemicals*. Van Nostrand-Reinhold, New York.
- Wilson, D.J., 1989. Soil clean up by in-situ surfactant flushing: I. Mathematical modeling. *Sep. Sci. Technol.* 24, 863–892.
- Wilson, D.J., Clarke, A.N., 1991. Soil clean up by in-situ surfactant flushing: IV. A two-compartment mathematical model. *Sep. Sci. Technol.* 26, 1177–1194.